Journal of Agricultural Engineering

https://www.agroengineering.org/

Design of attitude-adjustable chassis and dynamic stress analysis of key components for crawler combine harvester

Jinpeng Hu[1], Yang Yu[1,2,3], Tianle Ma[1], Peng Liu[1], Lizhang Xu[1,2,3]

1.College of Agricultural Engineering, Jiangsu University, Zhenjiang
2. Key Laboratory for Theory and Technology of Intelligent Agricultural Machinery and Equipment of Jiangsu University, Zhenjiang
3. Jiangsu Province and Education Ministry Co-sponsored Synergistic Innovation Center of Modern Agricultural Equipment, Zhenjiang, China

Please cite this article as doi: 10.4081/jae.2024.1685

Submitted: 24 June 2024
Accepted: 3 December 2024

Design of attitude-adjustable chassis and dynamic stress analysis of key components for crawler combine harvester

Jinpeng Hu[1], Yang Yu[1,2,3], Tianle Ma[1], Peng Liu[1], Lizhang Xu[1,2,3]

1.College of Agricultural Engineering, Jiangsu University, Zhenjiang
2. Key Laboratory for Theory and Technology of Intelligent Agricultural Machinery and Equipment of Jiangsu University, Zhenjiang
3. Jiangsu Province and Education Ministry Co-sponsored Synergistic Innovation Center of Modern Agricultural Equipment, Zhenjiang, China

Correspondence: Yang Yu, College of Agricultural Engineering, Jiangsu University, Zhenjiang, 212013, China
Email: yu_yang@ujs.edu.cn

Acknowledgements: This work was supported by the Jiangsu Province Agricultural Science and Technology Independent Innovation Fund Project (CX(24)3030); the 2023 Jiangsu Province Modern Agricultural Machinery Equipment and Technology Demonstration Promotion Project (NJ2023-04); the Jiangsu Graduate Research and Practice Innovation Program Project (KYCX22_3678); the Science and Technology Major Special Project of Anhui Province (202203a06020025) and Project of Faculty of Agricultural Engineering of Jiangsu University (NGXB20240202).

Contributions: JH, YY, TM, KC, PL, LX investigation; JH, TM, methodology; TM, PL, data curation; JH, TM, PL, test; JH, software, writing original draft; YY, conceptualization, writing, review and editing; YY, LX, funding acquisition, project administration. All the authors approved the final version to be published.

Conflict of interest: the authors declare no potential conflict of interest.

Keywords: crawler combine harvester; attitude adjusting mechanism; rigid flexible coupling; dynamic stress

Abstract

To address the issues of leveling difficulties and poor stability of crawler combine harvesters in hilly and mountainous regions, this research analyzed the mechanical causes of overturning instability in crawler combine harvesters and designed an omnidirectional attitude adjustment chassis based on a five-bar mechanism. A 3D model was developed in SolidWorks, and coupled rigid-flexible simulations were performed using RecurDyn. Results showed that the chassis could achieve an overall lift, lateral adjustments and longitudinal adjustments (0-100 mm, -5.18° to 5.55° and -4.06° to 5.15° respectively), with maximum dynamic stress occurring on the left front and left rear rotational arms. A dynamic stress testing system was established to conduct response surface experiments. Field test results revealed that the primary factors affecting the maximum stress of the left front rotational arm were the grain tank loading mass, lateral adjustment angle, and longitudinal adjustment angle. For the left rear rotational arm, the order was the longitudinal adjustment angle, lateral adjustment angle, and grain tank loading mass. Validation tests showed that at a lateral adjustment angle of 3.61°, a longitudinal adjustment angle of 3.20°, and a grain tank load of 350 kg, the average maximum stresses were 483.19 MPa for the left front rotational arm and 188.95 MPa for the left rear rotational arm, with corresponding structural safety factors of 1.61 and 4.31, meeting strength requirements. This work provides methods for optimizing the design and reliability testing of agricultural machinery chassis with attitude adjustment functions in hilly terrains.

Introduction

Traditional crawler combine harvesters generally weld the chassis frame and walking device into a single unit, providing good overall structural strength. However, this design limits the adjustment of the vehicle's attitude, adversely affecting maneuverability during harvesting. When the vehicle's tilt angle changes significantly, it can easily lead to tipping (Belinsky *et al.*, 2019; Sun *et al.*, 2020a). Therefore, it is necessary to adjust the level of the combine harvester during driving and operation to enhance operational efficiency, improve driving comfort, and reduce the likelihood of rollover accidents (Sirotin *et al.*, 2017).

Researches on leveling mechanisms and automatic leveling systems were mainly applied in engineering machinery and radar vehicles (İrsel and Altinbalik, 2018), with fewer applications in agricultural machinery. Some researchers have developed adjustable lifting chassis for combine harvesters and tractors (Liu *et al.*, 2018； Wang *et al.*, 2019; Hu *et al.*, 2022; Wang *et al.*, 2022; Lü *et al.*, 2024), primarily for wheeled machinery. These designs often add lifting mechanisms to fixed-clearance chassis, using hydraulic differential mechanisms or suspension structures on drive wheels to adjust ground clearance and achieve tilt compensation.

Compared to wheeled agricultural machinery chassis, there was less research on leveling technology for tracked chassis. Yang *et al.* (2014) proposed lateral and longitudinal leveling schemes using parallel four-bar and double-frame mechanisms, respectively, designing a remote-controlled omnidirectional leveling tracked tractor for mountainous areas, which can level on slopes up to 15° laterally and 10° longitudinally but was complex, required significant frame modifications, and lacked guaranteed structural strength and stability. Existing adjustable chassis designs for crawler harvesters typically had a tilt range of around 5°. Researchers like Sun *et al.* (2020), and Jin *et al.* (2020) provided similar design experiences, achieving a balance of adjustment effectiveness, structural reliability, and cost. More recent work by Paul *et al.* (2024) proposed a tracked chassis design based on a double-frame principle, allowing adjustment angles from 0° to 15°. However, this design only supported lateral adjustment and required a costly static hydraulic drive, resulting in a complex structure and significant modifications to the frame, which compromised strength and stability.

In order to improve the working performance of the lifting chassis, many scholars have conducted research on the adjustment performance and reliability of the lifting chassis. Sun *et al.* (2020a) conducted a static analysis of the frame and components such as the swing arm in a four-point lifting chassis using finite element software, optimizing the weak points in the design. Sun *et al.* (2020b) used finite element simulation to analyze the stress distribution and maximum stress locations of the active and passive swing arms in the attitude adjustment mechanism of a tracked tractor on slopes. Paul *et al.* (2024) used ANSYS software for numerical verification, confirming that the designed adjustable tracked harvester chassis had a maximum stress of 394 MPa and a safety factor of 1.94, meeting design requirements. However, most studies analyzed static conditions without considering the dynamic loads on the attitude adjusting mechanism during operations, which was crucial for assessing its reliability. RecurDyn multibody dynamics software models the dynamic behavior of rigid and elastic multibody systems, leveraging its integrated MFBD (Multi-Body Dynamics) technology for superior structural dynamic stress simulation. It has been effectively used in various engineering applications, including stress analysis of coal mining machine swing arms (Zhao *et al.*, 2023), flexible gear stress spectrum formulation for artillery steering systems (Si *et al.*, 2023) and UAV gimbal stability (Wang *et al.*, 2024). Given the limitations of traditional finite element methods in assessing the strength of chassis attitude adjustment mechanisms, RecurDyn simulations are poised to offer new insights and methodologies.

To achieve better attitude adjustment of the crawler combine harvester chassis and ensure its structural stability, this study validated the feasibility of the attitude adjustment mechanism based on the planar five-bar principle through theoretical derivation and multibody dynamics simulation. A virtual prototype model of the entire crawler combine harvester was constructed, and through rigid-flexible coupling simulation, the stress distribution and maximum stress locations of key components were extracted. Based on this, a prototype of the attitude-adjustable combine harvester was developed. Dynamic stress tests of key components were conducted under different lateral adjustment angles, longitudinal adjustment angles, and grain tank loadings to evaluate the structural strength of the chassis. This study aims to improve the reliability of the attitude-adjustable chassis of crawler combine harvesters and provide methods for the optimization design and reliability testing of agricultural machinery chassis.

Materials and Methods

Design of attitude adjustment device

Analysis of tipping stability of combine harvesters

Combine harvesters must navigate various terrains during field operations and transfers, emphasizing the importance of chassis stability. Lateral and longitudinal stability referred to the combine harvester's ability to resist tilting on slopes, primarily quantified by the critical tipping angle. On a slope (as illustrated in Figure 1), the harvester maintained moment equilibrium through various forces, including the machine's weight, the gravity acting on the traveling mechanism, the slope's supporting force, and friction. The maximum critical tipping angles for both lateral and longitudinal directions could be calculated using the formulas presented in Figure 1.

The parameters in Figure 1 were defined as follows: G_0 was the harvester's gravity; G_1 was the walking mechanism's gravity, *N*; N_1 and N_2 were the lateral slope's supporting forces, *N*; Z_1 and Z_2 were the friction forces, *N*; The maximum tilt angle that a crawler combine harvester did not tip over on the lateral slope was denoted as α_2, and the overturning moment was denoted as $\sum M_o$. B was the distance between the centres of the forces acting on the two tracks, mm; b was the width of a single track, mm; h_1 was the height of the vehicle's centre of gravity, mm; h_0 was the height of the centre of gravity of a single walking mechanism, mm; a was the distance from the centre of the front bearing wheel to the centre of gravity of the entire machine, mm; c is the distance from the centre of the rear bearing wheel to the centre of gravity of the entire machine, mm; l_1 was the distance from the resultant force N_3 to the contact point of the front bearing wheel, mm; l_2 was the distance from the resultant force N_4 to the contact point of the rear bearing wheel, mm; h was the height of the centre of gravity, mm; β was the angle of the longitudinal slope, ;° L was the distance between the centres of the front and rear bearing wheels.

Figure 1 demonstrated that the probability of tipping increased with steeper slope gradients. It was crucial to maintain the harvester's body as level as possible, regardless of whether it was positioned laterally or longitudinally on the slope. By adjusting the harvester's attitude, the relative positions of the lateral and longitudinal centers of gravity could be altered, thereby increasing the critical tipping angle. Consequently, the attitude adjustment mechanism in crawler combine harvesters could effectively enhance their resistance to tipping, thus improving overall stability.

Structural design of attitude adjustment mechanism

The diagram in Figure 2 illustrated the structure of the attitude-adjustable chassis, which comprised the crawler walking system, chassis frame, and attitude adjustment mechanism. To enable adjustment of the vehicle's attitude, the fixed beam typically used to connect the chassis frame with the two walking devices in traditional designs was eliminated. Instead, the upper frame of the chassis was designed as a fixed unit. Attitude adjustment was achieved through the symmetrical distribution of the attitude adjustment mechanism on each side, consisting of front rotational arms, connecting rods, rear arms, rear rotational arms, small rotational arms, front hydraulic cylinders, and rear hydraulic cylinders. On both sides, the front and rear rotational arms were rigidly connected through a central spline shaft to prevent relative displacement between the connecting mechanisms. The remaining connecting mechanisms were articulated to allow relative rotation.

Hydraulic adjustment system

The workflow diagram of the leveling hydraulic system was illustrated in Figure 3. The leveling hydraulic system primarily consisted of a fixed displacement pump, relief valve, switch valve, pressure compensator, electromagnetic proportional directional valve, hydraulic lock, shuttle valve, and hydraulic cylinders. In this system, FL and FR represented two lateral adjustment cylinders, while BL and BR denoted two longitudinal adjustment cylinders. WFL, WFR, WBL, and WBR represented electromagnetic proportional directional valves. The lateral leveling and overall lifting of the chassis were achieved when the fixed displacement pump 2 operated, switch valve 4 opened, electromagnetic proportional directional valves WFL and WFR activated, and hydraulic cylinders FL and FR actuated. Longitudinal leveling of the chassis was accomplished when the fixed displacement pump 2 operated, switch valve 4 opened, electromagnetic proportional directional valves WBL and WBR activated, and hydraulic cylinders BL and BR actuated.

The overall lifting and longitudinal adjustment of the chassis during the adjustment process required synchronous movement of the two rear and front cylinders in the system. However, the uneven weight distribution of the combine harvester itself led to an unbalanced load phenomenon in the hydraulic cylinders on both sides (Chai *et al.*, 2024), resulting in different flow rates entering the left and right hydraulic cylinders, thus producing synchronization errors.

During the height and longitudinal adjustments of attitude-adjustable chassis, synchronizing the rear and front hydraulic cylinders was crucial. However, the uneven weight distribution of the combine harvester caused asymmetric loading on these cylinders. Despite symmetrical positioning, traditional pumps and proportional valves controlling cylinder movements led to unequal flow rates due to varying loads, resulting in synchronization errors. These cumulative errors could cause chassis frame twisting, deformation, or even fractures, significantly reducing the lifespan of the adjustable chassis. Under the feedback action of shuttle valve 8, the spool of pressure compensator 5 automatically adjusted according to the outlet pressure of the proportional valve, consistently stabilizing the spool of the proportional valve in a balanced position. This maintained a constant pressure difference between the front and rear chambers of the proportional valve (Helian *et al.*, 2021). At this point, the output flow of the proportional valve was only related to the control current of the valve opening, thereby ensuring the same movement speed of the cylinders on both sides. Furthermore, this system allowed simultaneous opening of the four electromagnetic proportional directional valves of the chassis, but this was limited to the overall lifting and longitudinal adjustment actions of the chassis.

The attitude-adjustable chassis required appropriate ranges for height adjustment, lateral and longitudinal leveling. These features enabled it to adapt to more complex terrains by adjusting ground clearance and body posture, thereby improving the combine harvester's trafficability. This design aimed to avoid poor driving stability caused by an excessively raised center of gravity due to over-adjustment of vehicle height, as well as issues affecting the normal operation of main components due to excessive inclination adjustments. Based on the overall configuration parameters of the World 4LZ-4.0 crawler combine harvester, the structural characteristics and operational features of various working components supported by the chassis, and with reference to previous research, the main design parameters of the adjustable leveling chassis were preliminarily determined, as shown in Table 1.

Theoretical derivation of key adjustment parameters

Theoretical design of adjustment parameters

Based on the existing structure of the World 4LZ-4.0 crawler combine harvester chassis, the lengths and initial angles of each link were determined using graphical methods, while ensuring that the arrangement and adjustment requirements of the mechanism were met. The parameters of the components in the attitude adjustment mechanism were presented in Table 2.

The hydraulic cylinders in the chassis attitude adjustment mechanism determined the adjustment actions and ranges of the harvester's attitude through their combined extension and retraction. To analyze different adjustment conditions, mathematical models relating the chassis attitude to the extension of each hydraulic cylinder were established, aiding in the design of motion parameters for the adjustment mechanism's components and allowing for the assessment of the adjustment range. Additionally, based on the current attitude, the theoretical hydraulic cylinder adjustments can be derived, providing a control model for the automatic leveling system.

Height and lateral adjustment range of the chassis

As shown in Figure 4, the top view of the chassis defined the forward direction of the combine harvester as the Y -axis, with the X -axis perpendicular to it (ignoring changes in the Z -axis). When the harvester tilts laterally (around the Y -axis), the tilt angle was defined as the roll angle (β), and when it tilts longitudinally (around the X -axis), the tilt angle was the pitch angle (α). Points *B*, *M*, and *B'*, *M'* represented the hinge points of the adjustment mechanism and the frame.

During overall height adjustment, the left and right rear hydraulic cylinders remained in their initial positions, forming a parallelogram with points *ABMN* and *BDEM*, as shown in Figure 5. When the left and right front hydraulic cylinders extend simultaneously, the rear rotational arm rotated clockwise, raising point *M*. The height increase of the chassis was determined by the vertical height difference before and after the rotation of the arm *MN*, with theoretical calculations outlined in formulas (1)-(4). Based on the design requirement for overall chassis lift ranging from 0 to 100 mm, the length of front hydraulic cylinder *FG* was calculated to be between 400 mm and 465 mm, resulting in a ground clearance adjustment range of 255 mm to 355 mm.

$$h_D = L_{MN} \times (sin_{\theta_{MNA}} - sin_{\theta_{MNA_0}}) \tag{1}$$

$$\theta_{MNA} = \theta_{BMF} + \theta_{FMG} + \theta_{GMI} + \theta_{IMN} - 180° \tag{2}$$

$$\theta_{FMG} = cos^{-1}\frac{L_{FM}{}^2 + L_{GM}{}^2 - L_{FG}{}^2}{2 \times L_{FM} \times L_{GM}} \tag{3}$$

$$\theta_{GMI_0} = cos^{-1}\frac{L_{GM}{}^2 + L_{MI}{}^2 - L_{GI_0}{}^2}{2 \times L_{GM} \times L_{MI}} \tag{4}$$

In the formulas, h_D represented the height to which the chassis is raised, and L denoted the line connecting the rotation center points or endpoints of the components. θ_{MNA_0} was the initial angle of θ_{MNA}; θ_{BMF} and θ_{IMN} remained constant during posture changes. θ_{GMI_0} indicated the angle of θ_{GMI} in the horizontal position, and L_{GI_0} refered to the length of the rear hydraulic cylinder in the horizontal posture. During the overall elevation and lateral adjustments, the rear hydraulic cylinder did not participate, making θ_{GMI_0} a constant during attitude changes.

When the ground heights under the two tracks were inconsistent causing lateral tilt, lateral leveling operations were required. This adjustment can be understood as lowering the higher side or raising the lower side. As shown in Figure 6, when the left side was higher than the right, lateral leveling was achieved by raising the right side or lowering the left side. The mathematical relationship between the lateral tilt angle and the extension of the front hydraulic cylinder was given in formulas (5)-(7). The extension range of hydraulic cylinder *FG* (400 mm to 465 mm) resulted in a lateral tilt adjustment range of ±5.3°, aligning with the design requirements in Table 1.

$$\beta = tan^{-1}\frac{|H_R - H_L|}{B} \tag{5}$$

$$H_R = h_{DR} + H_0 \tag{6}$$

$$H_L = h_{DL} + H_0 \tag{7}$$

In the formulas, H_R and H_L represented the ground clearance of the right and left frame sides, respectively. B was the distance between the two walking beams. h_{DR} and h_{DL} indicated the changes in ground clearance after the left and right front hydraulic cylinders extend or retract, while H_0 was the initial ground clearance of the frame.

Longitudinal adjustment range of the chassis

In conditions where the front of the harvester was lower than the rear, as illustrated in Figure 7, the front side must be lowered. To achieve leveling during both forward and backward tilting, the rear hydraulic cylinders were designed to be initially extended to the same length. Given that forward tilting conditions were more common, the initial extension of the rear hydraulic cylinders was greater than their retraction. The mathematical relationship between the longitudinal tilt angle and the rear hydraulic cylinder extension was defined in formulas (8)-(18). Following the design experience of Sun *et al.*, with an initial installation distance of 385 mm, the length range of rear hydraulic cylinder L_{GI} was from 355 mm to 430 mm. This resultsed in a longitudinal tilt adjustment range of -2.9° to 5.2° (positive for forward tilt) at the lowest chassis position, and -4.1° to 4.6° at the highest position.

$$\alpha = \theta_{BMF} + cos^{-1}\frac{{L_{FM}}^2 + {L_{GM}}^2 - {L_{FG}}^2}{2 \times L_{FM} \times L_{GM}} + cos^{-1}\frac{{L_{GM}}^2 + {L_{MI}}^2 - {L_{GI}}^2}{2 \times L_{GM} \times L_{MI}} + \theta_{IMN} - \theta_{MNY} - 180° \tag{8}$$

$$\frac{L_{AM}}{\sin(\theta_{ANM})} = \frac{L_{AN}}{\sin(\theta_{AMN})} \tag{9}$$

$$\theta_{AMN} = cos^{-1}\frac{{L_{AM}}^2 + {L_{MN}}^2 - {L_{AN}}^2}{2 \times L_{AM} \times L_{MN}} = 360° - \theta_{AMB} - \theta_{BMF} - \theta_{FMG} - \theta_{GMI} - \theta_{IMN} \tag{10}$$

$$\theta_{AMB} = cos^{-1}\frac{{L_{AM}}^2 + {L_{XM}}^2 - {L_{AX}}^2}{2 \times L_{AM} \times L_{XM}} \tag{11}$$

$$L_{AM} = \sqrt{{L_{AX}}^2 + {L_{XM}}^2} \tag{12}$$

$$L_{XM} = L_{BM} - L_{AB} \times \cos(\theta_{ABM}) \tag{13}$$

$$L_{AX} = L_{AB} \times \sin(\theta_{ABM}) \tag{14}$$

$$\theta_{ABM} = \theta_{ABD} - \theta_{MBD} = \theta_{ABD} - 180° + \theta_{FMG} - \theta_{GME} + \theta_{FMB} \tag{15}$$

$$\theta_{ANO} = \frac{{L_{AN}}^2 + {L_{NO}}^2 - {L_{AO}}^2}{2 \times L_{AN} \times L_{NO}} \tag{16}$$

$$\theta_{YNO} = 180 - \theta_{AON} - \theta_{POA} \tag{17}$$

$$\theta_{AON} = \frac{{L_{AO}}^2 + {L_{NO}}^2 - {L_{AN}}^2}{2 \times L_{AO} \times L_{NO}} \tag{18}$$

In the formulas, *AX* represented the perpendicular line from *BM*, while θ_{BMF}, θ_{IMN} θ_{ABD}, and θ_{GME} were constant values during the attitude change process.

These theoretical calculations indicated that the theoretical lateral adjustment range was ±5.3°, the longitudinal adjustment range was -4.1° to 5.2°, and the height adjustment range was 0 to 100 mm, all meeting the overall design requirements outlined in Table 1.

Simulation of rigid flexible coupling of key components

Construction of simulation model

The front and rear rotational arms were the main components used to adjust the chassis attitude of the crawler combine harvester. During chassis adjustment, they bore the machine's weight and the driving load from the cylinders, as well as endured impacts from the frame and walking system, making them weak links in the adjusting mechanism. Therefore, analyzing the reliability of the front and rear rotational arms was necessary.

Using CAD software (Solidworks 2020, Dassault Systemes, Waltham, MA, USA), a tracked chassis attitude adjustment mechanism was designed. Simplified versions of the harvester's header, threshing, and cleaning systems were created to build a full-scale virtual prototype of the crawler combine harvester. This model was imported into RecurDyn (V9R5, FunctionBay Co., Seongnam, Korea), where the track module was added, and constraints and contacts between the adjustment mechanism, frame, and walking beam were established. The harvester's weight was added to the frame according to actual operating conditions. The terrain model, based on real working scenarios, included flat ground, laterial slope β, and longitudinal slope α, with relevant parameters shown in Figure 8. For slope adjustments, considering safety and the operability for operators and test personnel, we chose the slow gear of the harvester in our research. The harvester moved slowly at a forward speed of 0.8 m/s.

After establishing the rigid body model of the combine harvester, the front and rear rotational arms were meshed using Hypermesh (Version 2021, Altair Engineering, Troy, MI, USA) and imported into the tracked mechanism model, replacing the original rigid swing arms. This completed the rigid-flexible coupled model. The mesh quantities and material properties of the swing arms and other components are shown in Table 3 (Zhou *et al.*, 2024).

After establishing the rigid-flexible coupled model of the crawler combine harvester with the rotational arms, the flexible body of the rotational arms was divided into patches to enable contact with the rigid frame. FDR elements were used to create pin holes in the flexible body of the rotational arms to facilitate force transmission between the flexible and rigid bodies (Adams and Darr, 2022; Wu *et al.*, 2023). The final rigid-flexible coupled model of the tracked chassis was established, as shown in Figure 9.

Verification of the theoretical adjustment model

To verify the working principle of the adjustable chassis, simulations of the vehicle's attitude adjustment under various conditions were conducted. The hydraulic cylinder actuation was achieved through designated driving functions. During overall lifting and longitudinal adjustment, the height and pitch angle of the chassis were recorded, as shown in Figures 10 and 11.

From Figure 11, it was evident that from 0 to 3s, both front hydraulic cylinders extended by 65 mm while the rear cylinders remained unchanged, resulting in a total lift of 100 mm. When at the maximum height, the front cylinders held steady while the rear cylinders retracted by 30 mm, achieving a maximum rear tilt angle of -4.24°. The rear cylinders then extended by 75 mm, reaching a maximum forward tilt of 5.00°. Between 22 and 25 s, the front cylinders retracted by 65 mm, returning the chassis to its lowest position, while the rear cylinders repeated the previous actions, achieving longitudinal tilt limits of -2.2° and 5.35°. This analysis indicated that simultaneous adjustment of the front cylinders facilitated overall lifting, while the rear cylinders enabled longitudinal adjustments, with a height adjustment range of 0 to 100 mm and a longitudinal tilt range of -4.24° to 5.35°.

The simulation results for lateral tilt adjustment, shown in Figure 13, demonstrated that the left and right mechanisms were identical. Focusing on right tilt as an example, the left front cylinder extended by 65 mm from 0 to 4 s, reaching a maximum lateral adjustment angle of -5.53° at the 4-second mark. A similar left tilt adjustment achieved a maximum angle of 5.25°. The simulation results revealed that the established dynamic model for the attitude-adjustable chassis exhibited some discrepancies in longitudinal and lateral adjustment ranges compared to theoretical predictions. These differences were attributed to track sinkage, affecting the pressure distribution between the tracks and the ground, consistent with findings by Sun *et al* (2020). Overall, the simulation confirmed that the adjustment actions aligned with theoretical designs, and the adjustment ranges met theoretical calculations.

Dynamic stress analysis of typical working conditions

Based on this, a rigid-flexible coupled analysis was conducted for typical walking conditions of the combine harvester, and the average dynamic stress of the rotational arms during stable phases was extracted. This simulation considered the effects of dynamic loads such as track walking systems and machine weight on stress variations and was performed under maximum lateral and longitudinal adjustment conditions, as shown in Figures 12 a,b.

The typical adjustment conditions for the chassis attitude adjustment include left tilt, right tilt, overall lifting, forward tilt, and backward tilt. Simulations were conducted for each condition to obtain dynamic stress contour maps of key components, as shown in Figure 13. By combining Figure 13 a-c, it can be observed that in the lateral adjustment condition of the chassis, the stress distribution of the front rotational arms on both sides is similar. However, the left rotational arm experienced higher stress, with the maximum stress area located near the hinge position between the left front arm and the connecting rod, identified as the maximum stress area 1 in the figure.

The stress distribution of the rear rotational arms was influenced by the specific adjustment conditions. Under left tilt and synchronized lifting, the left rear arm experienced higher stress, while in right tilt, the right rear arm bore slightly higher stress than the left, though both remained within the range of 120-150 MPa. The maximum stress area for the rear arms was located near the pivot axis of the rear arm and the fixed area of the rear connecting arm, denoted as maximum stress area 2 in the figure. This disparity in stress distribution was attributed to the combine harvester's centre of gravity being closer to the left side, resulting in different loads on the two sides of the mechanism.

Figure 13 d,e indicated that during longitudinal adjustment, the rear arms experienced significantly lower stress compared to the front arms. This was attributed to a higher concentration of weight at the front, leading to increased stress in the front arms. The maximum stress area for the front arms remained near area 1. Despite the weight disparity between the chassis sides, the maximum stress area for the rear arms remained at area 2, with the left rear arm experiencing higher stress than the right.

Based on the results of the rigid-flexible coupled simulation, it was found that the stress amplitudes of the arm components were relatively large under left tilt and forward tilt conditions. The maximum stress positions were located at area 1 of the left front arm and area 2 of the left rear arm. Across the five extreme adjustment conditions, the maximum stress range at area 1 varied from 280 to 324 MPa, while at area 2, it varied from 122 to 140 MPa. These results can serve as reference values for the installation of strain gauges and the verification of structural strength in subsequent stress tests.

Prototype construction and dynamic stress testing

Construction of prototype

Based on the simulation results, adjustment angles and vehicle weight were identified as the primary factors affecting stress on the front and rear rotational arms, with left tilt and forward tilt conditions being particularly significant. To investigate the impact of these factors on the structural strength of the arms, we identified the maximum stress distribution locations. A prototype crawler combine harvester with attitude adjustment capabilities was then constructed, and dynamic stress testing experiments were conducted.

The crawler combines harvester prototype consisted of an attitude adjustment mechanism, hydraulic valve group, tilt sensor, onboard controller, and manual operation panel, as shown in Figure 14. The tilt sensor (MQJS30V1CC, Milang Technology Co., Shenzhen, China) had a maximum output frequency of 100 Hz and a dynamic measurement accuracy of 0.02°. It was mounted on the chassis frame below the cab to measure lateral and longitudinal tilt. The displacement sensor (WY-01-100, Milang Technology Co., Shenzhen, China) connected to the hydraulic cylinder to monitor its extension and provide feedback to the controller for limit protection. The onboard controller (RC28-14, Bosch Rexroth, Germany) managed communication, sensor integration, and issued hydraulic cylinder adjustment commands.

Test location and conditions

The experiments were conducted in the rice test field at the College of Agricultural Engineering, Jiangsu University. Based on prior simulations and the allowable angle range for the crawler combine harvester operating on slopes, the lateral adjustment range was set to a left tilt of 0-5° and the longitudinal adjustment range to a forward tilt of 0-5°. During the actual field tests, the slopes with both lateral and longitudinal inclines were artificially created. Considering that weight changes during actual harvesting primarily result from variations in grain load in the tank, the weight loading range for the grain tank during the experiment was determined to be 0-350 kg, based on the actual capacity of the 4LZ-4.0 combine harvester's grain tank.

Dynamic stress testing method

Dynamic stress was monitored and recorded during chassis adjustment using standard 45° triaxial strain gauges and a dedicated resistance strain gauge instrument (Han *et al.*, 2022; Li *et al.*, 2016). These gauges measured strain in three directions, allowing for the calculation of principal stress with high accuracy. Strain gauges were affixed to the maximum stress areas of the front and rear arms and connected to the DH5902N dynamic stress measurement system. The maximum stress values of the left front arm and left rear rotational arm were measured under different parameters with a sampling frequency of 500 Hz. The dynamic stress measurement setup was shown in Figure 15.

Design of response surface experiment

This study employed the Box-Behnken response surface optimization method to conduct a three-factor and three-level response surface experiment. Experimental design was performed using Design-Expert 13.0 software. The selected factors were lateral adjustment angle β, longitudinal adjustment angle α, and grain tank loading mass m, with the corresponding response variables being the maximum stress of the left front rotational arm y_1 and the left rear rotational arm y_2. The design factors and levels were presented in Table 4.

Results and Discussion

Validation of the actual adjustment effects

The validation of the actual adjustment effects was carried out through measured data for lateral adjustment and overall lift height (Figure 16). As shown in Figure 17, the displacement of the rear hydraulic cylinders remained constant. In the first 15s, the displacement of the two front cylinders changed by 65 mm, resulting in a maximum ground clearance of approximately 100 mm for the chassis, confirming the overall lift height range of 0 to 100 mm. From 15 to 28 s, with only the left front cylinder extending 65 mm, the chassis tilted to the right at a maximum angle of 5.15°; from 30 to 42s, with only the right front cylinder extending 65 mm, the chassis tilted to the left at a maximum angle of 5.55°. Thus, the lateral adjustment range for the adjustable chassis was -5.18° to 5.55°, with the differences in the extreme adjustment angles likely due to actual processing and assembly errors.

The longitudinal adjustment measured data was shown in Figure 18. During the first 22s, when the extension of both front hydraulic cylinders was 0 mm, the chassis was at its lowest position. At this time, the rear cylinders synchronously changed by -30 to 45 mm, resulting in a longitudinal angle change range of -3.13° to 5.15°. From 25 to 42s, when the extension of both front cylinders was 65 mm, the chassis was at its highest position. The rear cylinders synchronously changed by -30 to 45 mm, resulting in a longitudinal angle change range of -4.06° to 4.55°. Therefore, the longitudinal adjustable range for the adjustable chassis was -4.06° to 5.15°.

Taking the dynamic stress changes of the left front and left rear arms during the synchronous lift of the chassis as an example, the dynamic stress test curve was shown in Figure 19. Figure 19 indicated that the stress variation curve displayed oscillations, primarily due to the polygon effect generated during the tracked movement. During the posture holding phase, the stress curve was relatively stable, with the average stress in this phase serving as the maximum stress for the arms. Each stress measurement was taken five times for averaging. The maximum stress values obtained from the strain gauges at the bonded locations across various conditions were compared with the average stress values in the corresponding regions of the simulation model, resulting in an error range of 5% to 7%. This indicated that the maximum stress locations obtained from the rigid-flexible coupling simulation model were reasonable and could meet the testing requirements for subsequent experiments.

Analysis of variance of test results

The experimental scheme and dynamic stress results were shown in Table 5, with the ANOVA of the results in Table 6. Here, A represented the coded value of the chassis lateral adjustment angle α, B represented the chassis longitudinal adjustment angle β, and C represented the grain tank loading mass m.

Based on the ANOVA results in Table 5, for the dynamic stress of the left front rotational arm, factors A, B, C, AB, and BC were all significant, while the lack-of-fit value was 0.2390, not significant relative to the pure error. The predictive R^2 of 0.9482 was consistent with the adjusted R^2 of 0.9887, with a difference of less than 0.2, indicating a high fit of the regression equation. The signal-to-noise ratio was 47.025, greater than 4, showing good predictive performance of the regression equation. The factors' influence on the maximum stress of the left front swing arm was: grain tank loading mass > lateral adjustment angle > longitudinal adjustment angle. The regression equation after removing the non-significant terms was as follows:

$$\begin{aligned} y_1 = 218.83 + 10.82A + 27.88B + 0.17C - 1.50AB - 0.02BC \\ - 3.24B^2 + 0.01C^2 \end{aligned} \tag{19}$$

Based on the ANOVA results in Table 6, for the dynamic stress of the left rear rotational arm, factors A, B, C, AC, and BC were all significant, while the lack-of-fit value was 0.6713, not significant relative to the pure error. The predictive R^2 of 0.9984 was consistent with the adjusted R^2 of 0.9962, with a difference of less than 0.2, indicating a high fit of the regression equation. The signal-to-noise ratio was 59.374, greater than 4, showing good predictive performance. The factors' influence on the maximum stress of the left rear swing arm was: longitudinal adjustment angle > lateral adjustment angle > grain tank loading mass. The regression equation after removing the non-significant terms was as follows:

$$\begin{aligned} y_2 = 30.72 + 58.18A + 15.84B + 0.62C + 0.02AC - 0.04BC \\ - 10.79A^2 - 0.01C^2 \end{aligned} \tag{20}$$

Analysis of the interaction between different factors

The interaction effects of various factors on the stress of the left front rotational arm were shown in Figure 20. In Figure 20a, when the grain tank loading mass was constant, a significant interaction between the lateral adjustment angle and the longitudinal adjustment angle was observed. Both angles had a notable impact on the stress of the left front rotational arm. The maximum stress of the left front rotational arm gradually increased with both the lateral and longitudinal adjustment angles, with the lateral adjustment angle having a greater influence on the stress amplitude.

From Figure 20b, it was observed that when the longitudinal adjustment angle was constant, there was an interaction between the lateral adjustment angle and the grain tank loading mass, but the interaction was not significant. Both the lateral adjustment angle and the grain tank loading mass significantly affected the stress of the left front rotational arm. The maximum stress of the left front rotational arm increased with both the lateral adjustment angle and the grain tank loading mass, with the grain tank loading mass having a greater influence on the stress amplitude.

From Figure 20c, it was observed that when the lateral adjustment angle was constant, there was a significant interaction between the longitudinal adjustment angle and the grain tank loading mass. Both angles significantly affected the stress of the left front rotational arm. The stress increased with both the longitudinal adjustment angle and the grain tank loading mass. The effect of the grain tank load variation was more significant compared to the maximum stress variation caused by the longitudinal adjustment angle.

The interaction effects of various factors on the stress of the left rear rotational arm were shown in Figure 21. From Figure 21a, it was observed that when the grain tank loading mass was constant, there was an interaction between the lateral adjustment angle and the longitudinal adjustment angle, but the interaction was not significant. Both the lateral adjustment angle and the longitudinal adjustment angle significantly affected the stress of the left rear rotational arm, with the longitudinal adjustment angle being more significant. The stress initially increased and then decreased with an increase in the lateral adjustment angle, showing significant fluctuations. As the longitudinal adjustment angle increased, the stress gradually increased, with a relatively stable change.

From Figure 21b, it was observed that when the longitudinal adjustment angle was constant, there was a significant interaction between the lateral adjustment angle and the grain tank loading mass. Both significantly affected the stress of the left rear rotational arm, with the lateral adjustment angle being more significant. The stress initially increased and then decreased with increases in both the lateral adjustment angle and the grain tank loading mass, showing significant fluctuations.

From Figure 21c, it was observed that when the lateral adjustment angle was constant, the longitudinal adjustment angle and grain tank loading mass significantly affected the stress of the left rear rotational arm, with a significant interaction between the two. The longitudinal adjustment angle was more significant. Stress increased with both the longitudinal adjustment angle and grain tank loading mass, but the variation in grain tank load caused significant stress fluctuations. The variation in the longitudinal adjustment angle led to a more gradual change in stress.

Based on the experimental results, the dynamic stress regression equations were used to determine the maximum stress during the adjustment process. The parameters found were: a lateral adjustment angle of 3.61°, a longitudinal adjustment angle of 3.20°, and a grain tank loading mass of 350 kg. Under these conditions, the maximum stress for the left front rotational arm and the left rear rotational arm were 473.52 MPa and 198.10 MPa, respectively. According to the calculated maximum stress results, five validation tests were conducted using the specified parameters. The average maximum stress for the left front rotational arm and the left rear rotational arm were 483.19 MPa and 188.95 MPa, respectively. The error between the test averages and the predicted values was within 5%, validating the regression prediction model. In mechanical design, a safety factor greater than 1.5 is typically required to ensure proper operation (Amirafshari *et al.*, 2021; KARLIŃSKI *et al.*, 2023). Using the measured average maximum stresses, the strength of the components was checked, as shown in formulas (21) and (22).

$$S_1 = \frac{\delta_s}{y_{1max}} = \frac{780}{483.19} = 1.61 > 1.5 \tag{21}$$

$$S_2 = \frac{\delta_s}{y_{2max}} = \frac{780}{188.95} = 4.13 > 1.5 \tag{22}$$

In summary, we concluded that the designed arm structures met the strength requirements. However, it is noteworthy that the safety factor for the left rear rotational arm was nearly three times the design requirement, indicating an overdesign in material and structural parameters. Future work can focus on optimizing the material selection and structural design of this component to balance manufacturing costs, weight, and strength. Additionally, operators should avoid operating the combine harvester with chassis adjustment at maximum stress conditions for the front and rear rotational arms. This practice reduces the risk of failure, such as fractures in the adjustment mechanism, thereby extending the lifespan of the combine harvester.

Conclusion and future work

This research mainly carried out the following innovative work:

(1) An analysis was conducted on the mechanical reasons for the tilting instability of a crawler combine harvester, and a chassis attitude adjustment device based on a planar five bar mechanism was proposed, which can achieve overall lifting (0-100mm), lateral adjustment (-5.18° -5.55°), and longitudinal adjustment (-4.06° -5.15°) of the chassis.

(2) A rigid-flexible coupling simulation model of a crawler combine harvester was constructed, and the stress distribution status and maximum stress position of key components of the attitude adjustment mechanism during the attitude adjustment process were determined. A prototype of a crawler combine harvester with chassis adjustment function was developed, and a dynamic stress testing system was built.

(3) Orthogonal regression experiments were conducted using lateral adjustment angle, longitudinal adjustment angle, and grain tank loading mass as experimental factors, and maximum stress on the left front and left rear rotational arms as experimental indicators. The results indicated that the main and secondary factors affecting the maximum stress of the left front rotational arm were: grain tank loading

mass, lateral adjustment angle, and longitudinal adjustment angle. The order of factors affecting the maximum stress of the left front rotational arm was: longitudinal adjustment angle, lateral adjustment angle, and grain tank loading mass. By solving the regression equation, it was found that when the lateral adjustment angle was 3.61 °, the longitudinal adjustment angle was 3.20 °, and the loading mass of the grain tank loading mass was 350kg, the maximum stress of the left front and left rear arms were 473.52 MPa and 198.10 MPa, respectively, with safety factors of 1.61 and 4.31.

(4) The safety factor verification results of the key components of the attitude-adjustable chassis indicated that both meet the strength requirements, verifying the accuracy of the rigid flexible coupling model. The research can further provide support and basis for the optimization design of the chassis structure.

However, in addition to the conventional adjustment conditions discussed in this study, extreme scenarios such as overloading and obstacle crossing also need attention, as excessive impact loads can cause fractures and failures in weak structural components of the chassis. Due to the risks associated with testing under these extreme conditions, we currently lack the necessary facilities. Importantly, this paper has established and validated a coupled rigid-flexible simulation model, which can effectively simulate and analyze more complex scenarios. Moving forward, we will conduct further tests and improvements on chassis reliability under extreme conditions using the developed prototype and stress collection system.

References

Adams, B., Darr, M. 2022. Validation principles of agricultural machine multibody dynamics models. J. ASABE 65:801-814.

Amirafshari, P., Brennan, F., Kolios, A. 2021. A fracture mechanics framework for optimising design and inspection of offshore wind turbine support structures against fatigue failure. Wind Energy Sci 6:677-699.

Belinsky, A., Ziganshin, B., Valiev, A., Haliullin, D., Galiev, I., Adigamov, N. 2019. Theoretical investigation of increasing efficiency of combine harvester operation on slopes. Eng.f Rural Develop. 18:206-213.

Chai, X., Hu, J., Ma, T., Liu, P., Shi, M., Zhu, L., Xu, L. 2024. Construction and characteristic analysis of dynamic stress coupling simulation models for the attitude-adjustable chassis of a combine harvester. Agronomy (Basel) 14:1874.

Jin, C., Yang, T., Liu, G., Wang, t., Chen, M., Liu, Z. 2020. Design and test of posture controlled chassis for caterpillar combine. Trans. CSAE 51:393-402.

Han, J., Kim, E., Moon, S., Lee, H., Kim, J., Park, Y. 2022. Fatigue integrity assessment for tractor-mounted garlic-onion harvester. J. Terramech. 100:1-10.

Helian, B., Zheng, C., Bin, Y. 2021. Energy-saving and accurate motion control of a hydraulic actuator with uncertain negative loads. Chin. J. Aeronaut. 34:5:253-

264.

Hu, J., Pan, J., Dai, B., Chai, X., Sun, Y., Xu, L. 2022. Development of an attitude adjustment crawler chassis for combine harvester and experiment of adaptive leveling system. Agronomy (Basel) 12:717.

İrsel, G., Altinbalik, M. T. 2018. Adaptation of tilt adjustment and tracking force automation system on a laser-controlled land leveling machine. Comput. Electron. Agric. 150:374-386.

Karliński, J., Stańco, M., Działak, P. 2023. The impact of the driving conditions on stress of load-bearing structure of self-propelled electric mining machine. Mater. Today Pro. 9: 791-798.

Li, F., Liu, S., Mao, E., Du, Y., Lin, Y., Tian, J. 2016. Fatigue analysis of corn harvester frame based on power density. Trans. Chin. Soc. Agric. Eng. 32:34-40.

Lü, X., Liu, Z., Lü, X., Wang, X. 2024. Design and study on the leveling mechanism of the tractor body in hilly and mountainous areas. J. Eng. Design Technol. 22:679-689.

Paul, A., Machavaram, R. 2024. Design of an adjustable chassis for a track type combine harvester. Cogent Eng. 11:2353811.

Sirotin, P., Zhileykin, M., Sapegin, A., Zlenko, S. 2017. Prerequisites for the creation of an integrated system for leveling and cushioning framework of combine harvesters. Tract. Agr. Machin. 84: 21-28.

Sun, J., Meng, C., Zhang, Y., Chu, G., Zhang, Y., Yang, F., Liu, Z. 2020. Design and physical model experiment of an attitude adjustment device for a crawler tractor in hilly and mountainous regions. Inform. Process. Agric. 7:466-478.

Sun, Y., Xu, L., Jing, B., Chai, X., Li, Y. 2020. Development of a four-point adjustable lifting crawler chassis and experiments in a combine harvester. Comput. Electron. Agric. 173:105416.

Si, D.Y., Fang, W.M., Zhang, Y. 2023. Flexible gear modeling and stress spectrum compilation of an artillery steering machine. J. Phys. Conf. Ser. 2528:012001.

Wang, Y., Yang, F., Pan, G., Liu, H., Liu, Z., Zhang, J. 2014. Design and testing of a small remote-control hillside tractor. J. ASABE 57:363-370.

Wang, Z., Ma, W., Wang, T., Liu, C. 2022. Body leveling control model establishment and experiment analysis. Appl. Eng. Agric. 38: 243-251.

Wang, Z., Xia, Y. 2019. Model establishment of body attitude adjustment system based on Backstepping control algorithm and automatic leveling technology. Cluster Comput. 22:14327-14337.

Wang, Z., Yang, J., Liu, P., Long, X., Li, H., Wei, W. 2019. Development of an agricultural vehicle levelling system based on rapid active levelling. Biosyst. Eng. 186:337-348.

Wu, G., Wang, S., Zhang, A., Xiao, Y., Li, L., Yin, Y., Yan, B. 2023. Optimized design and experiment of a self-covering furrow opener for an automatic sweet potato seedling transplanting machine. Sustainability (Basel) 15:13091.

Wang, C.J., Liu, Q., Yang, L. 2024. The MFBD-DEM coupling simulation approach for the investigation of granules screening effi-ciency in 4-DOF flip-flow screen. Granul. Matter. 26:5.

Zhao, L.J., Yang, S.J., Zhang, H.N., Han, L.G. 2023. Fatigue life prediction of shearer rocker shell based on DEM-MFBD bidirec-tional coupling technology. Coal Sci. Tech. 51:S252-258.

Zhou, B., Chen, S., Hu, J., You, Y., Wang, D., Zhang, Q. 2024. Multi-body dynamics modeling and test of an articulated steering half-track tractor. Int. J. Agric. Biol. Eng. 16:124-133.

Table 1 Main technical parameters of attitude-adjustable chassis

Items	Parameters
Load capacity /kg	3500
Grounding length of the track /mm	1240
Width of the track /mm	350
Track gauge /mm	1080
Lateral adjustment range /°	±5
Longitudinal adjustment range /°	-4~5
Maximum lifting height /mm	100

Table 2 The rod length and initial angle of the attitude adjustment mechanism

Items	Parameters	Items	Parameters
L_{ON}/mm	90	L_{ME}/mm	100
L_{AB}/mm	270	L_{BM}/mm	1075
L_{BD}/mm	100	L_{AO}/mm	1022.4
L_{DE}/mm	1075	θ_{MNA_0}/°	11.46
L_{MN}/mm	270	θ_{BMF}/°	19.42
L_{MI}/mm	355	θ_{IMN}/°	35
L_{GM}/mm	163.4	θ_{ABD}/°	145
L_{GI_0}/mm	385	θ_{GME}/°	22.03

Table 3. Material and mesh properties of flexible rotational arms

Items	Parameters	Items	Parameters
Material	40Cr	Grid size /mm	10
Young's modulus /GPa	206	Number of nodes of the front rotational arm	4788
Poisson ratio	0.29	Number of units of the front rotational arm	16314
Density/g/cm3	7.85	Number of nodes of the rear rotational arm	3863
Yield strength /MPa	780	Number of units of the rear rotational arm	12327

Table 4. Experimental factors and levels

Test codes	Lateral adjustment angle β /°	Longitudinal adjustment angle α /°	Grain tank loading mass m /kg
-1	0	0	0
0	2.5	2.5	175
1	5	5	350

Table 5. Response surface test scheme and test results

Test number	Lateral adjustment angle β /°	Longitudinal adjustment angle α /°	Grain tank loading mass m /kg	Average stress of left front rotational arm /MPa	Average stress of left rear rotational arm /MPa
1	0	5	175	318.25	143.22
2	2.5	5	0	286.957	189.51
3	0	2.5	350	401.052	92.175
4	5	5	175	365.218	191.13
5	0	0	175	266.855	101.04
6	2.5	0	0	256.31	107.745
7	0	2.5	0	268.375	68.865
8	5	2.5	0	327.294	97.59
9	2.5	5	350	410.248	201.93
10	5	0	175	351.443	139.29
11	2.5	2.5	175	337.269	210.36
12	2.5	2.5	175	334.267	210.045
13	2.5	2.5	175	338.352	217.98
14	2.5	2.5	175	347.567	209.73
15	2.5	0	350	411.768	187.245
16	5	2.5	350	473.252	160.845
17	2.5	2.5	175	341.278	211.05

Table 6. Analysis of variance of response surface test results

Key components	Source of variance	Total variance	Degree of freedom	Mean square deviation	*F value*	*P value*	Significance
Left front rotational arm	Model	52923.22	9	5880.358	155.9032	<0.0001	**
	A	8624.769	1	8624.769	228.6646	<0.0001	**
	B	1111.491	1	1111.491	29.46844	0.001	**
	C	38834.62	1	38834.62	1029.604	<0.0001	**
	AB	353.8161	1	353.8161	9.380564	0.018252	*
	AC	44.09624	1	44.09624	1.169103	0.315422	
	BC	258.679	1	258.679	6.858237	0.034468	*
	A^2	148.2476	1	148.2476	3.93042	0.087854	
	B^2	1724.67	1	1724.67	45.72537	0.000262	**
	C^2	2003.389	1	2003.389	53.11492	0.000164	**
	Residual	264.026	7	37.718			
	Lack of fit	162.4127	3	54.13758	2.131122	0.239022	
	Pure error	101.6133	4	25.40332			
	Sum	53187.25	16				
Left rear rotational arm	Model	41449.46585	9	4605.496	472.0906	<0.0001	**
	A	4211.554753	1	4211.555	431.7092	<0.0001	**
	B	4534.852613	1	4534.853	464.8492	<0.0001	**
	C	3982.111903	1	3982.112	408.19	<0.0001	**
	AB	23.3289	1	23.3289	2.39135	0.165929	
	AC	398.9007563	1	398.9008	40.88968	0.000369	**
	BC	1124.9316	1	1124.932	115.3121	<0.0001	**
	A^2	19156.297	1	19156.3	1963.634	<0.0001	**
	B^2	2.135250592	1	2.135251	0.218876	0.654114	
	C^2	6573.923385	1	6573.923	673.866	<0.0001	**
	Residual	68.28874875	7	9.755536			
	Lack of fit	20.10076875	3	6.700256	0.556177	0.671269	
	Pure error	48.18798	4	12.047			
	Sum	41517.7546	16				

P<0.05 indicates significant; P<0.01 indicates very significant

Critical conditions for lateral tipping:

$$\left\{\begin{aligned} &\sum M_o = N_2(B+0.5b) + G_0 sin\alpha \cdot h_0 + 2G_1 sin\alpha \cdot h_1 - G_0 cos\alpha(0.5B+0.5b-e) - G_1 cos\alpha(B+b) = 0 \\ &N_2 = [G_0 cos\alpha(0.5B+0.5b-e) + G_1 cos\alpha(B+b) - G_1 sin\alpha \cdot h_0 - 2G_1 sin\alpha \cdot h_1] \\ &\alpha \le arctan\left[\frac{(G_0+2G_1)(0.5B+0.5b) - G_0 e}{G_0 \cdot h_0 + 2G_1 \cdot h_1}\right] \end{aligned}\right\}$$

Critical conditions for longitudinal tipping:

$$\left\{\begin{aligned} &(cG_0 + 2LG_1)cos\beta - (G_0 h_1 + 2G_1 h_0)sin\beta - N_3(L - l_1 - l_2) = 0 \\ &N_3 = \frac{(cG_0 + 2LG_1)cos\beta - (G_0 h_1 + 2G_1 h_0)sin\beta}{(L - l_1 - l_2)} \ge 0 \\ &\beta \le arctan\frac{G_0 h_1 + 2G_1 h_0}{cG_0 + 2LG_1} \end{aligned}\right\}$$

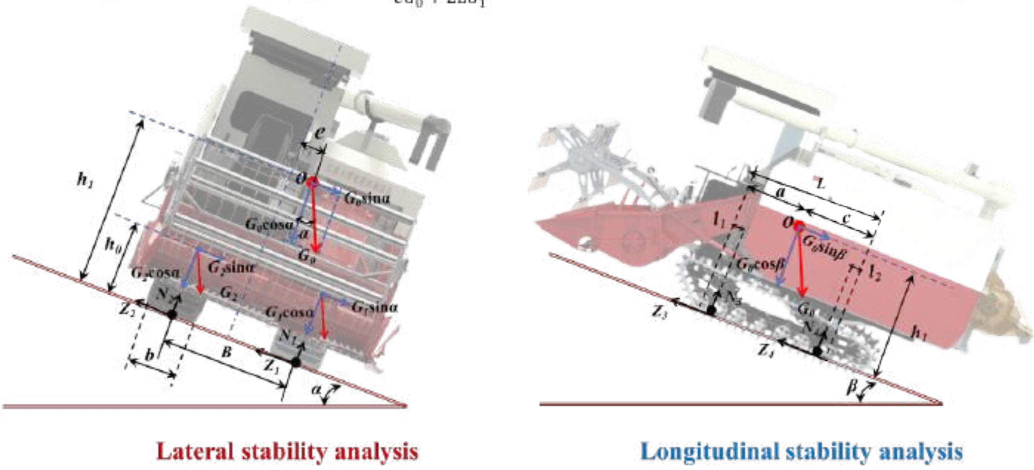

Figure 1. Lateral and longitudinal stability analysis of crawler combine harvester

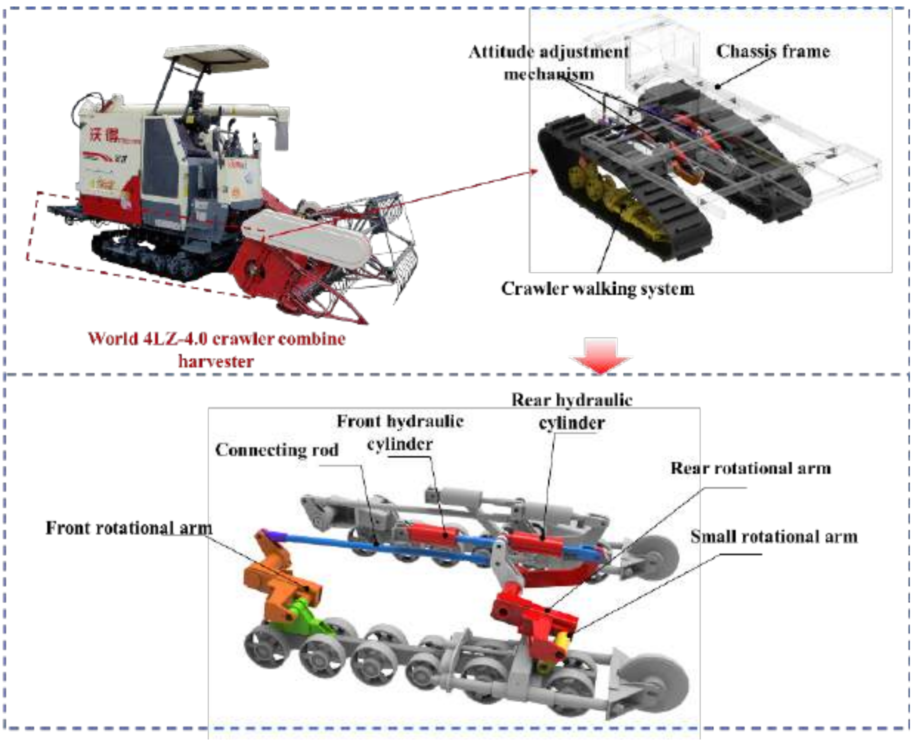

Figure 2. Chassis attitude adjustment structure of crawler combine harvester

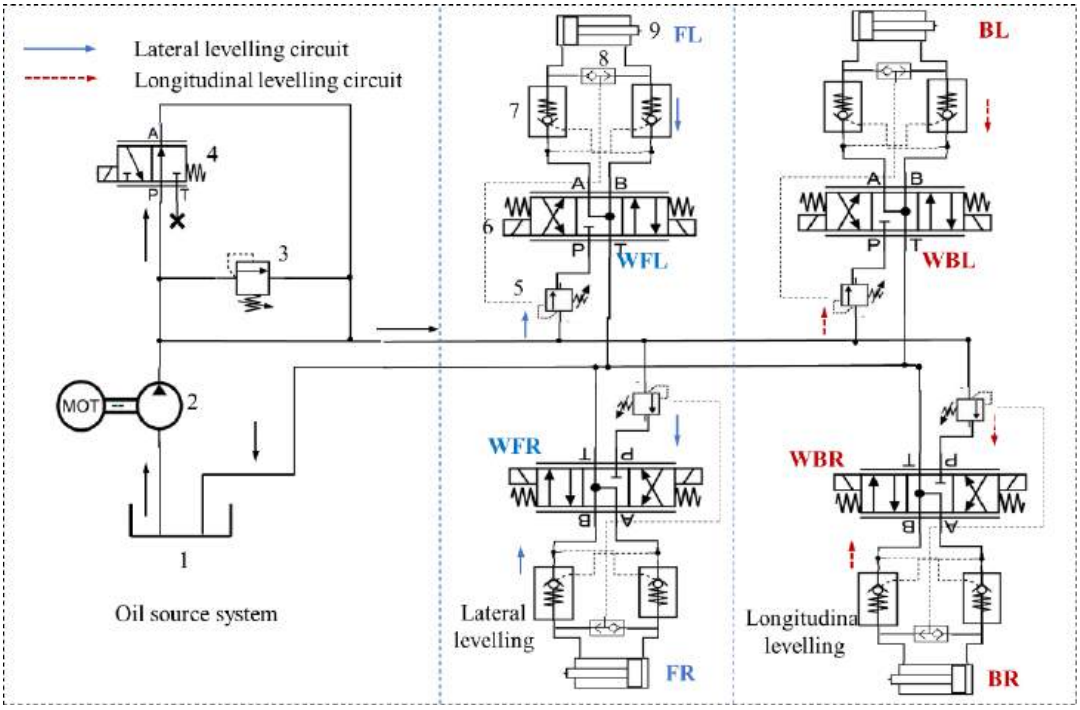

Figure 3. Hydraulic system of attitude-adjustable chassis: (1) hydraulic tank;(2) fixed displacement pump; (3) relief valve; (4) switching valve; (5) pressure compensator; (6) proportional directional valve; (7) hydraulic lock; (8) shuttle valve; (9) hydraulic cylinder

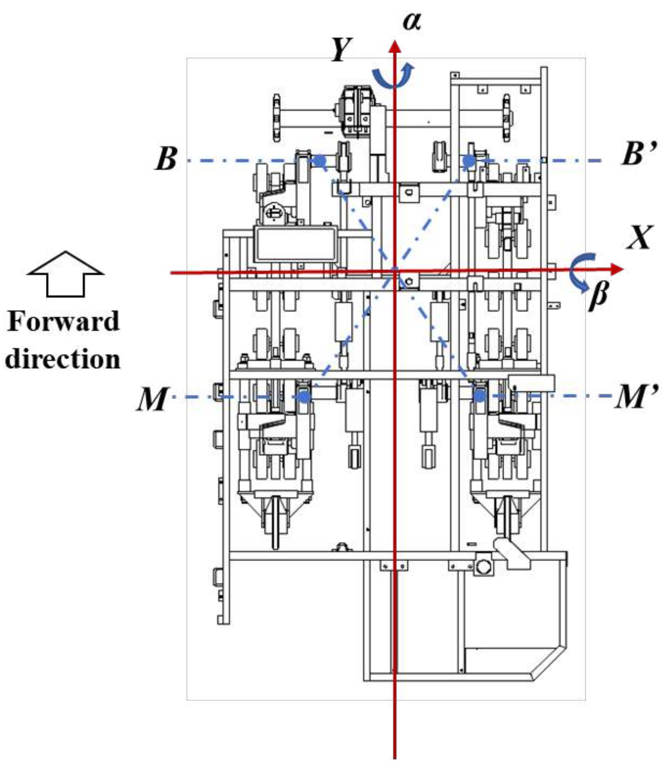

Figure 4. Definition of chassis coordinate system and tilt direction

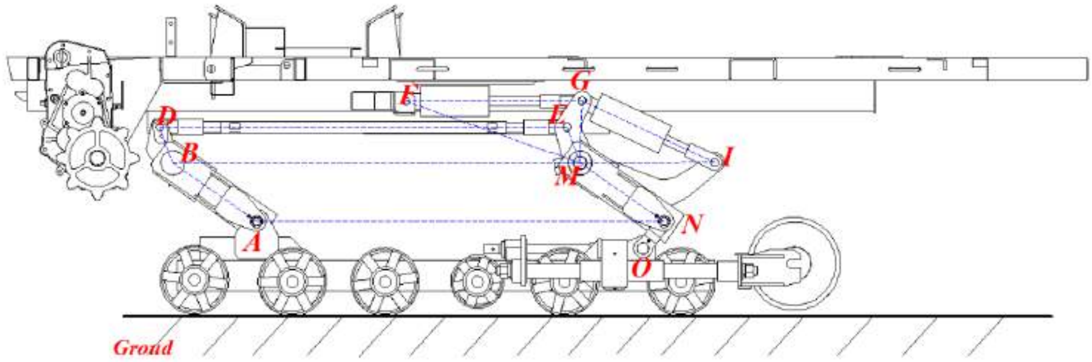

Figure 5. Geometric model of overall lifting working conditions

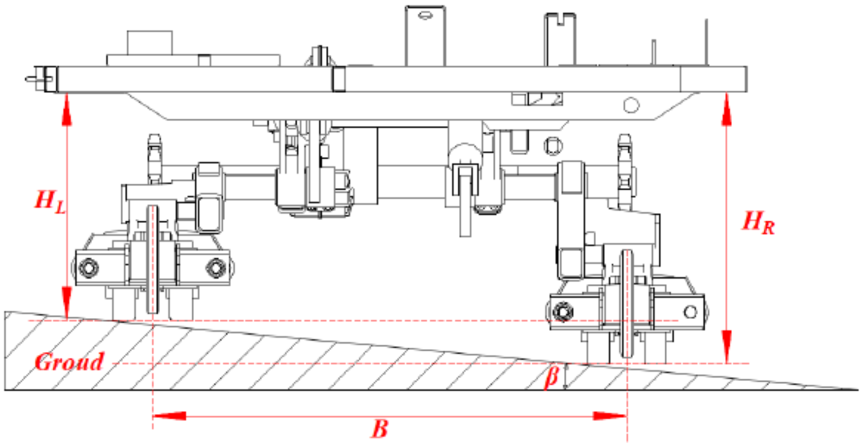

Figure 6. Geometric model of lateral adjustment working condition

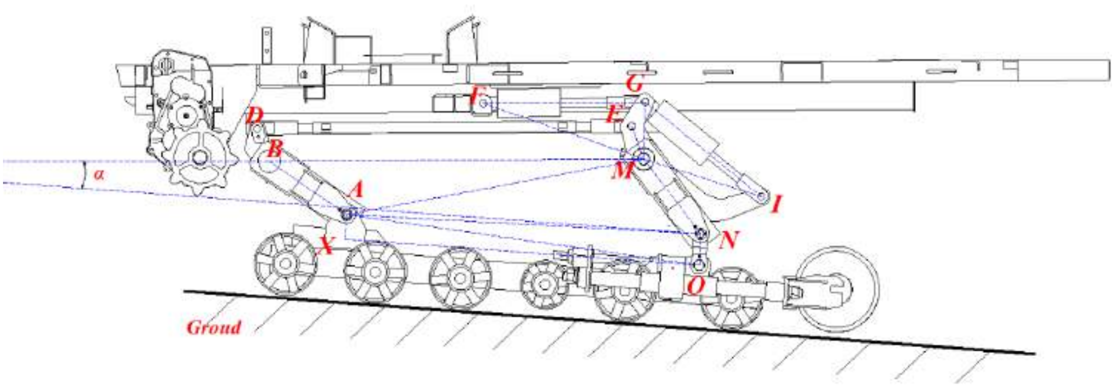

Figure 7. Geometric model of longitudinal adjustment working condition

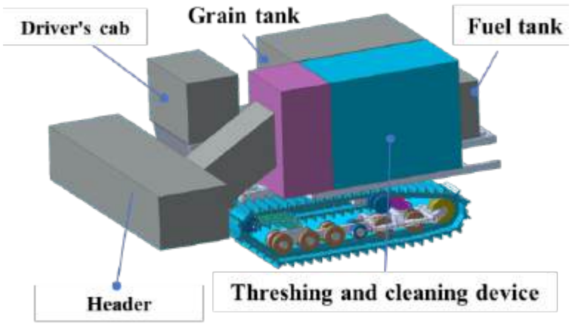

(a) Simplified combine harvester model

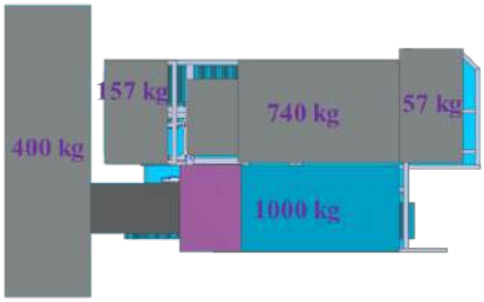

(b) Overall weight distribution

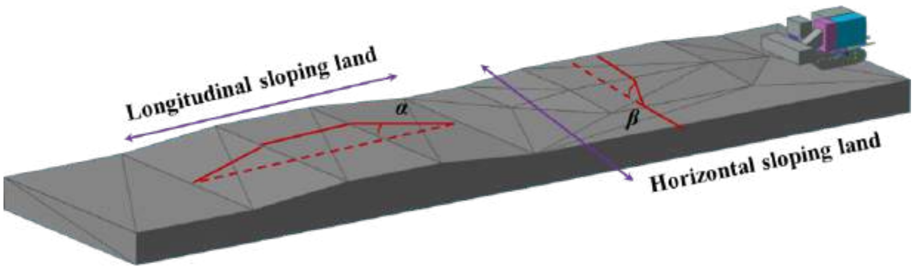

(c) Simulation model of ground

Figure 8. Virtual prototype model of crawler combine harvester

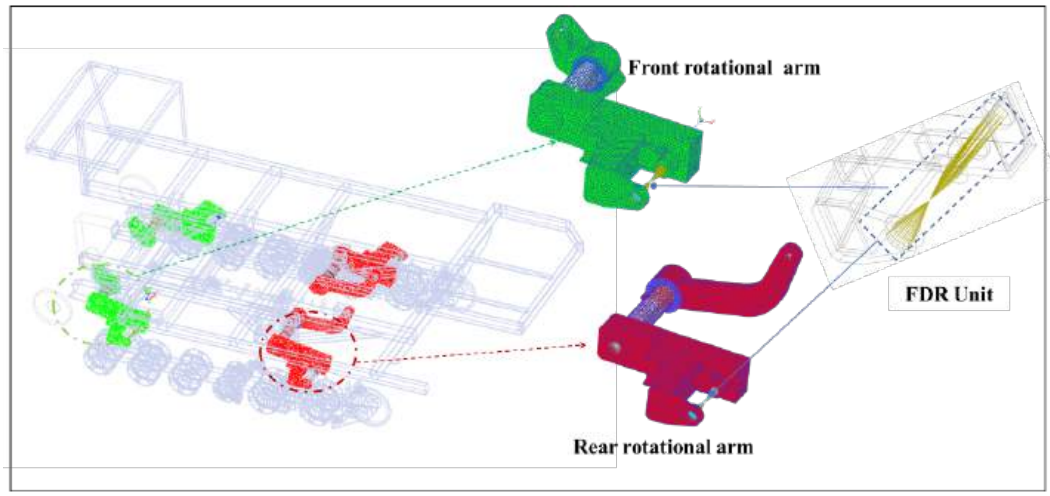

Figure 9. Rigid-flexible coupling model of front and rear arms

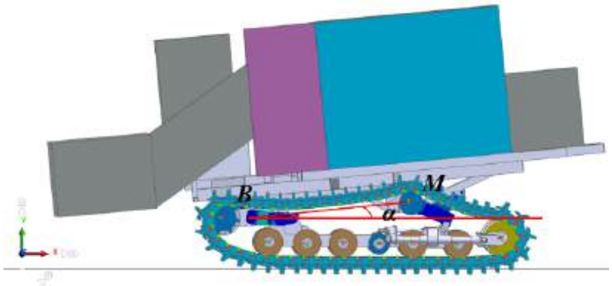

(a) Forward tilting process of chassis

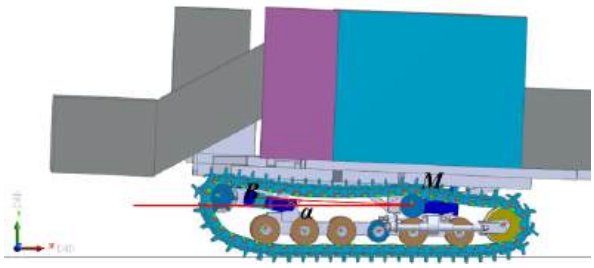

(b) Backward tilting process of chassis

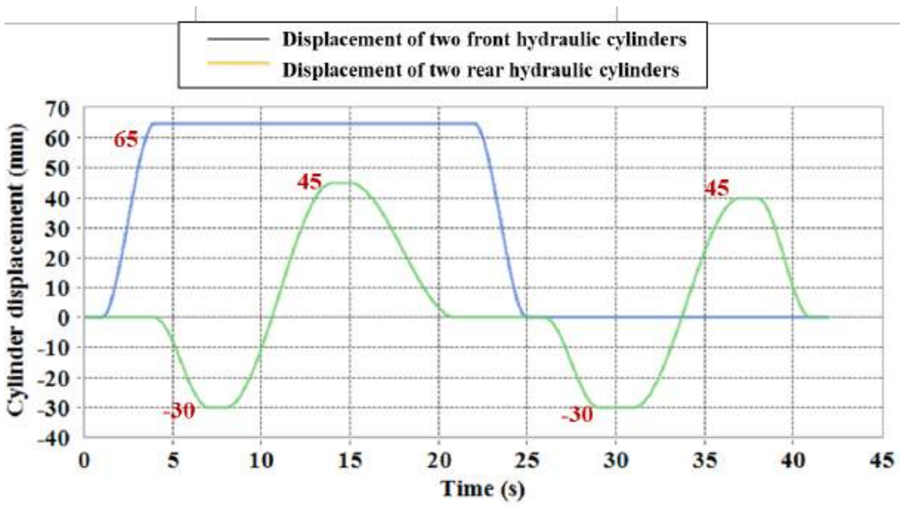

(c) Displacement changes of the front and rear cylinders

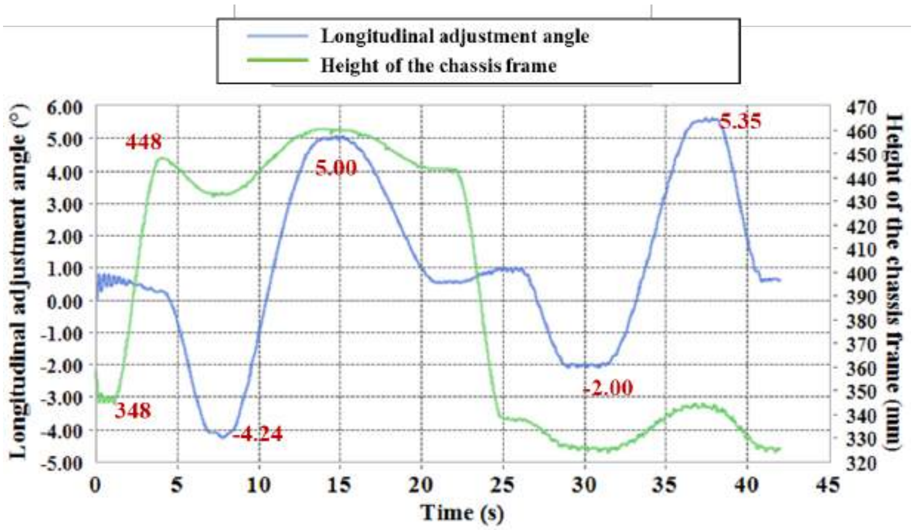

(d) Longitudinal angle changes of the crawler harvester.

Figure 10. Simulation results of longitudinal adjustment

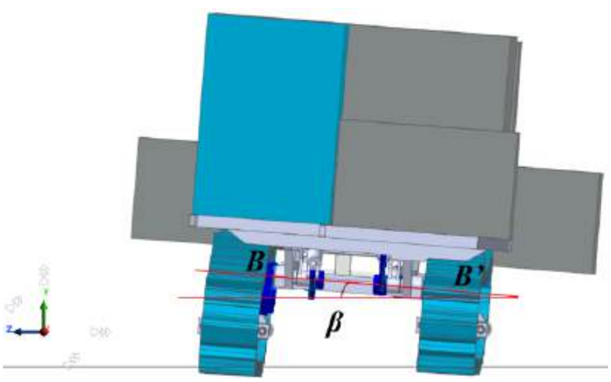

(a) Right tilting process of chassis

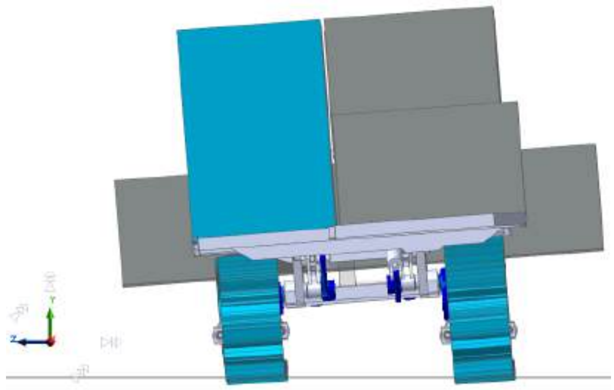

(b) Left tilting process of chassis

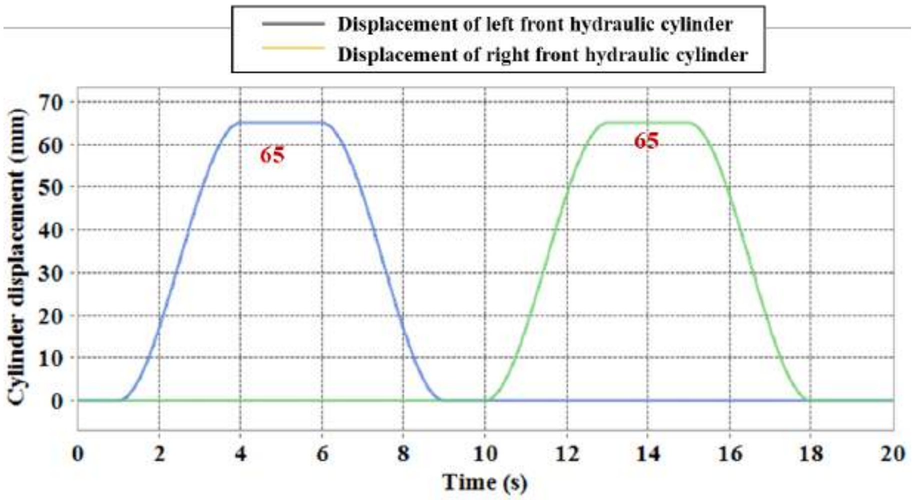

(c) Displacement changes of the front cylinders

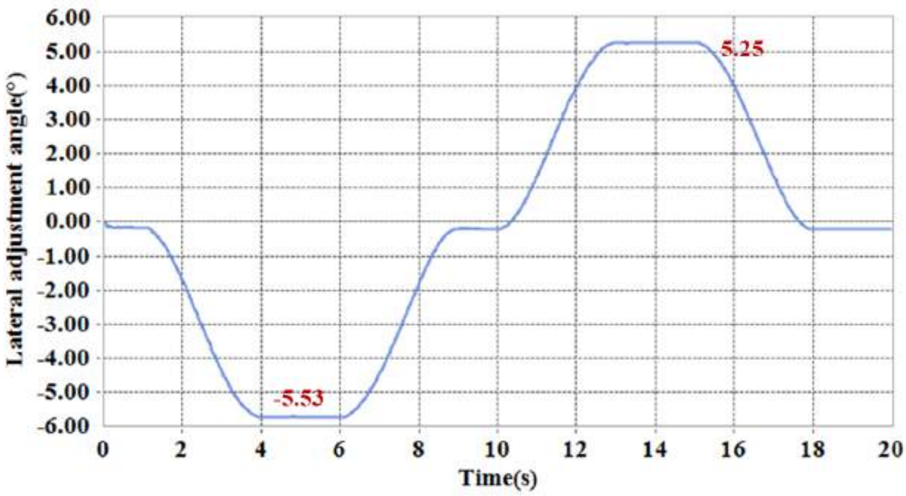

(d) Lateral angle changes of the crawler harvester

Figure 11. Simulation results of lateral adjustment

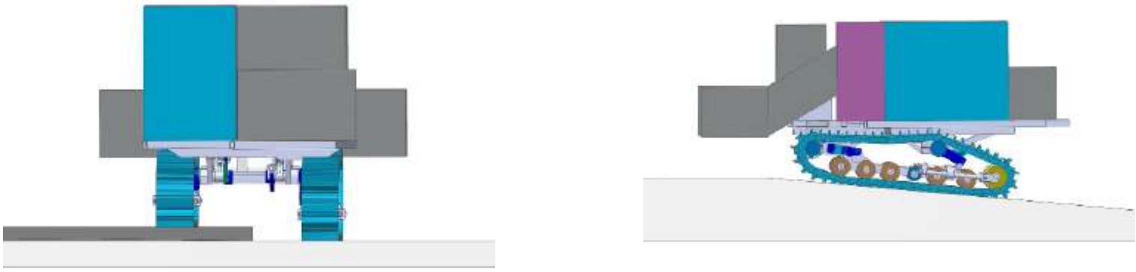

(a) Lateral adjustment simulation (b) Longitudinal adjustment simulation

Figure 12. Rigid-flexible coupling simulation of attitude adjustable chassis

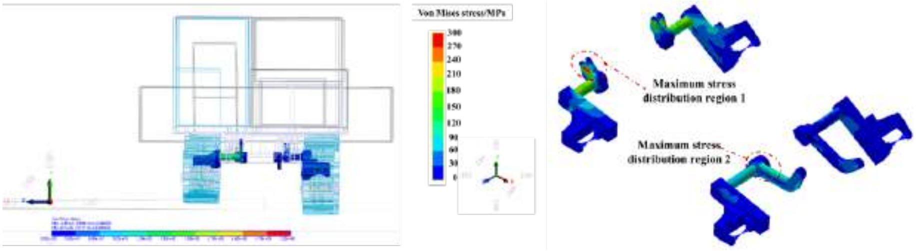

(a) The stress distribution of the rotational arms under the maximum left tilt leveling condition

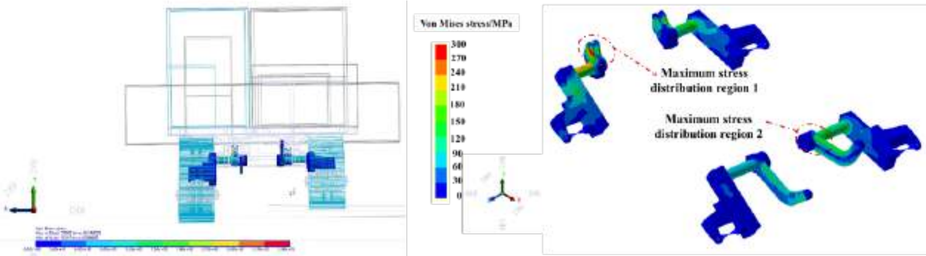

(b) The stress distribution of the rotational arms under the maximum right tilt leveling condition

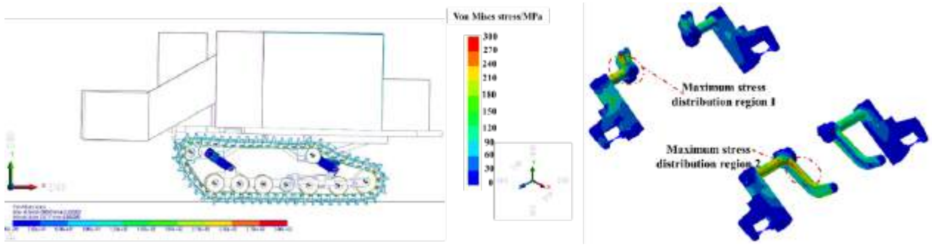

(c) The stress distribution of the rotational arms under the maximum lifting condition

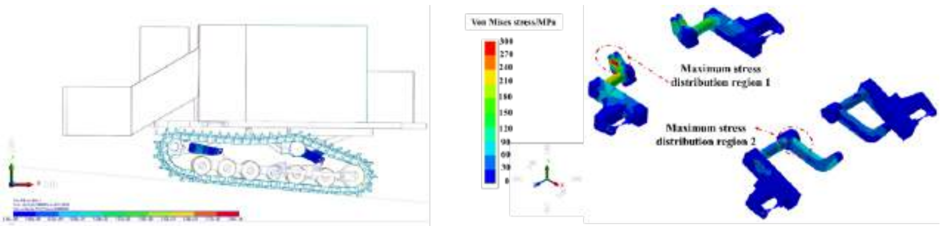

(d) The stress distribution of the rotational arms under the maximum forward leveling condition

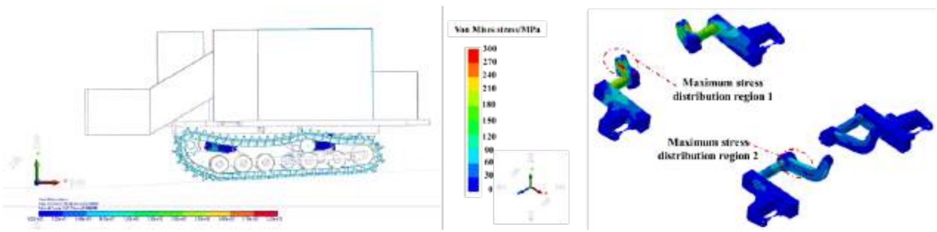

(e) The stress distribution of the rotational arms under the maximum backward tilt leveling condition

Figure 13. Dynamic stress cloud diagram of key components under typical working conditions

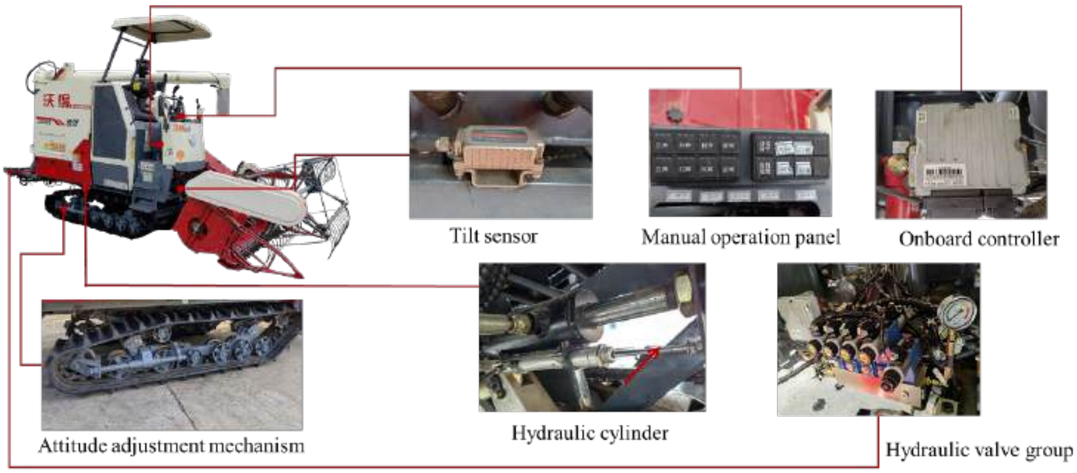

Figure 14. System integration of attitude adjustment chassis prototype

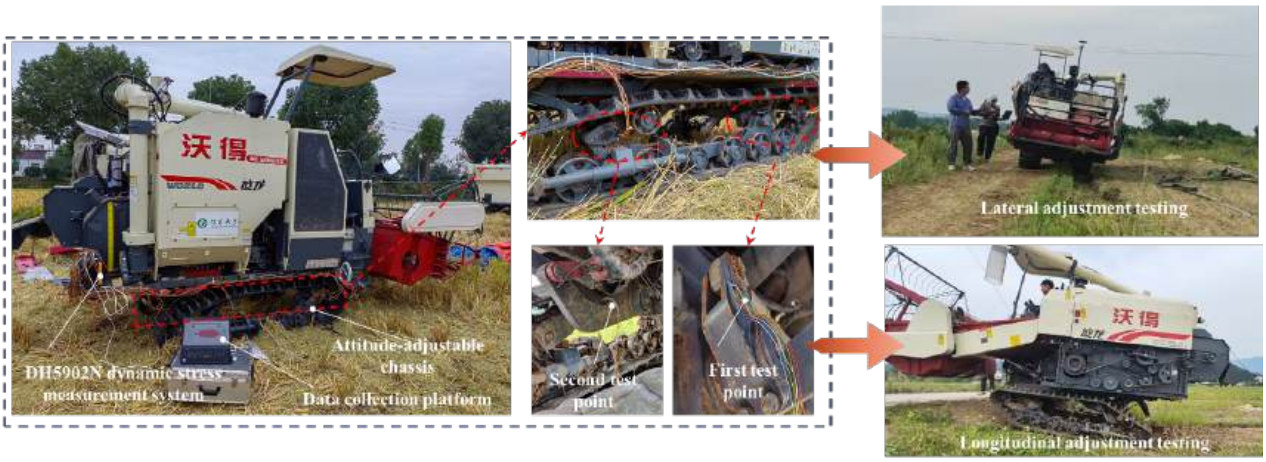

Figure 15. Dynamic stress test site of attitude adjustment mechanism

(a) Actual lateral adjustment scenario in the field (b) Actual longitudinal adjustment scenario in the field

Figure 16. Cylinder displacement and adjustment angle data measuring on-site

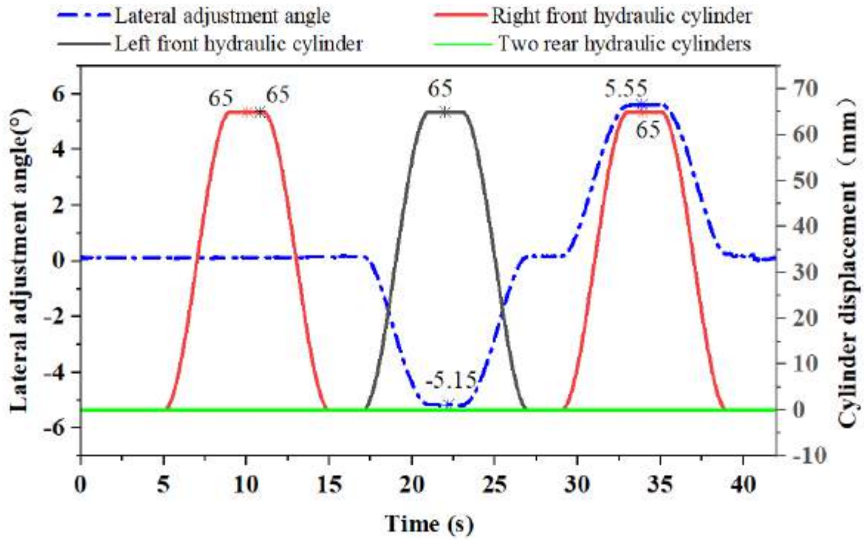

Figure 17. Measured data of lateral adjustment angle, overall lifting height, and cylinder displacement.

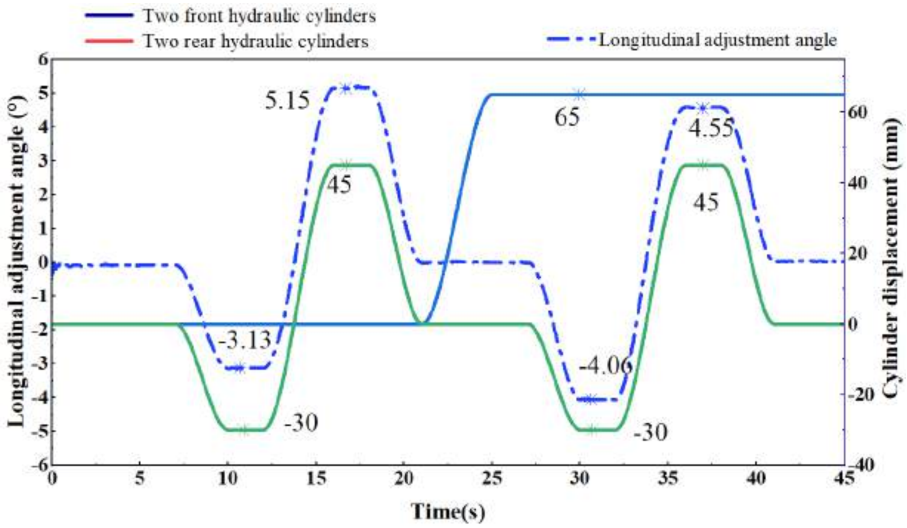

Figure 18. Measured data of longitudinal adjustment angle and cylinder displacement

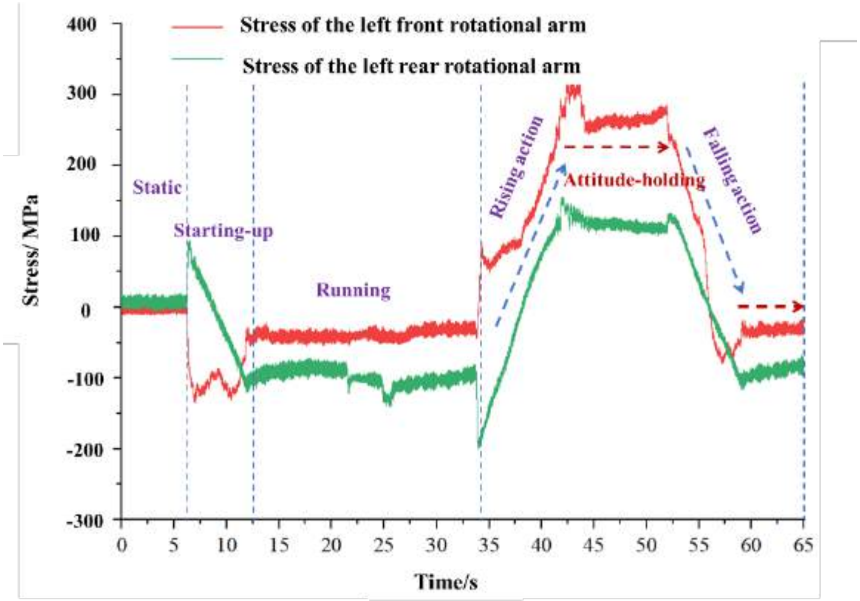

Figure 19. Dynamic stress curve of the left front and rear rotational arms during the lifting of the chassis

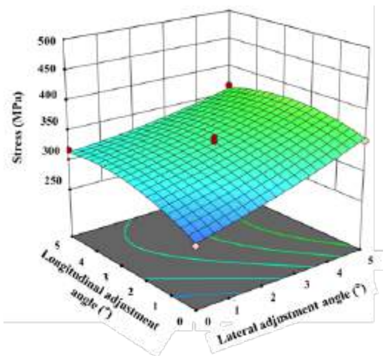

(a) Interaction between longitudinal and lateral adjustment angle

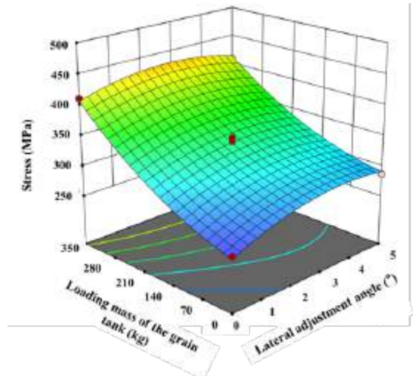

(b) Interaction between loading mass of the grain tank and lateral adjustment angle

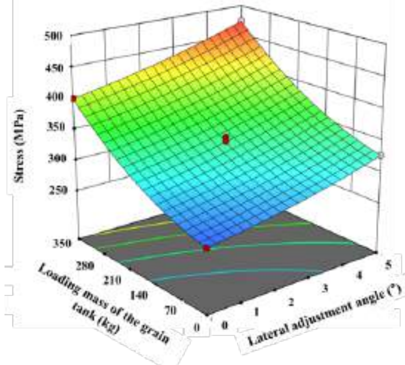

(c) Interaction between lateral adjustment angle and loading mass of the grain tank

Figure 20. The interaction of various factors on the stress of the left front rotational arm

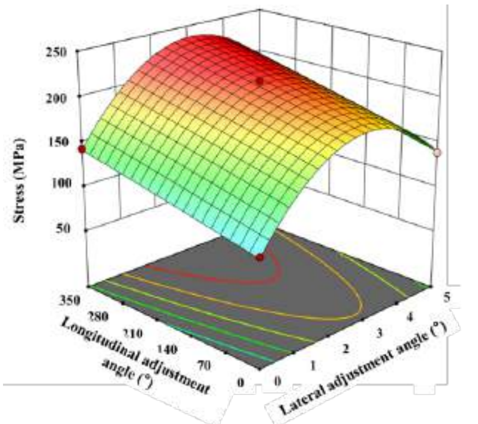

(a) Interaction between longitudinal and lateral adjustment angle

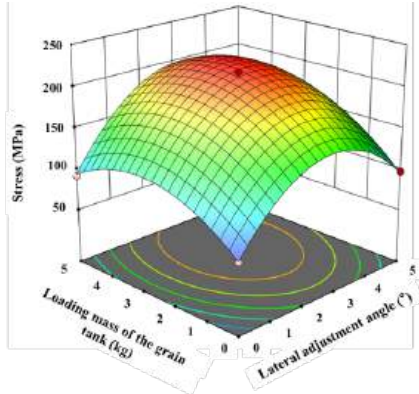

(b) Interaction between lateral adjustment angle and loading mass of the grain tank

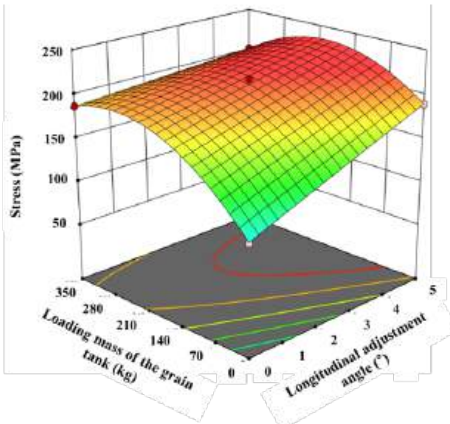

(c) Interaction between longitudinal adjustment angle and loading mass of the grain tank

Figure 21. The interaction of various factors on the stress of the left rear rotational arm